ISSN 1330-3651 (Print), ISSN 1848-6339 (Online)
https://doi.org/10.17559/TV-20221206142059
Preliminary communication

Kinematics Analysis and Simulation of Biped Transportation Robot in Stair Climbing Scene

Zhen Yu TANG, Qi Lin BI*, Xue Min NING, Lun TANG, Minling LAI, Jindong YU

Abstract: Difficult and labour-intensive transportation up and down the steps is a challenge in small spaces. This work focused on the smooth performance requirements about each joint structure of robot foot. We have made research on the hand and foot structure of the transport part, which simplifies its posture calculation in the designed bipedal transport robot model. Methods for determination of each joint angle of the hand and foot are presented, including the use of standard D-H method to establish a mathematical model and perform forward and inverse kinematic analysis to derive the angles of each joint, where the matrix was coded by Python software to ensure the accuracy of the calculated results. The joints angles are assigned by the Step function, and the motion of the bipedal robot in the case of single access is simulated by the inverse kinematic derivation formula. Simulation results show that the structure of the robot's joints meets the requirement of maintaining the stability of the robot when going up and down the stairs.

Keywords: bipedal robot; handling; kinematic analysis; simulation

1 INTRODUCTION

With the progress of science and technology the application of intelligent mobile robots is more and more common. Research on bionic service robots is flourishing in China and abroad [1-4]. While most handling robots are oriented to the service industry and are mainly used for planar mobile transportation, it is hard to realize flexible handling in some non-planar scenes such as going up stairs and climbing slopes. For example, the traditional wheeled and tracked conveying robots have the characteristics of poor obstacle surmounting ability, poor terrain adaptability, low turning efficiency, large turning radius, easy slipping and instability, which leads to limited application. The crawler type handling machine is extreamly demanding on the terrain, it is not capable of handling terrain with large differences in height. The double-handling machine can adapt to almost all kinds of complex terrain. It can cross obstacles with good freedom, flexibility, freedom of movement and stability. Therefore, a bipedal handling robot applied in people's life can not only meet the demand for convenient handling, but also ensure personal safety of the handler [5]. Research on bionic design service-oriented robots is also flourishing in China and abroad [1, 6].

Taking a common life delivery robot as an example, this paper analyzes the main building blocks and drives required for the robot [7]. The analysis of the robot's hand structure, foot structure and motion posture is implemented by combining the location of handling and the size of the items to be carried [8-10]. The hand and foot structure of the bipedal handling robot is designed with the bionic human hand and foot structure, and the designed parts are subjected to force verification and finite element static stress-strain analysis of the key parts structure, which makes the parts rationalized, reliable and practical [11]. On the basis of the conclusion that the maximum deformation of key parts is within 0.016 mm , the maximum stress in rated condition is within 149 MPa, which is within the allowable range of the material, further research will be conducted later.

The design of a service robot needs to take into account the mechanical structure and the corresponding kinematic posture. It is essential to carry out the practical strengthening of the motion on the existing structural model based on the structural bionic design and analysis of the bipedal handling robot, to ensure the feasibility of the robot design, where the kinematics is divided into positive and inverse kinematics [12].

2 COMPOSITION AND ANALYSIS OF BIPEDAL HANDLING ROBOTS

The human hand structure mainly consists of the wrist, palm and fingers. The finger joint has only one degree of freedom, so it can only perform flexion and extension. The wrist movements have two degrees of freedom; the wrist mainly performs flexion and extension movements to change the overall direction of the hand [13]. The human foot consists mainly of the thigh, knee, calf, ankle, and foot. Considering the main lifting factors of handling, the fingertips must not touch the ground when the hand is perpendicular to the horizontal line of the ground (designed parameters are shown in Fig. 1) [12-16]. The bipedal handling robot system designed in this paper can be divided into the control system, drive system (braking system), monitoring and sensing system, support skeleton, deceleration system, and shock absorption system, where the support skeleton mainly consists of four parts: head, hand, body, and foot (as shown in Fig. 2). For the bionic design mechanism, the joints are directly driven by electricity [17], and the material is selected from 6061 aluminum alloy [18].

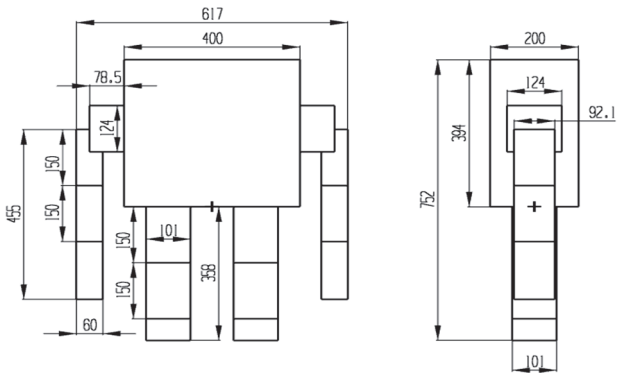

Figure 1 Main parameters of the bipedal handling robot

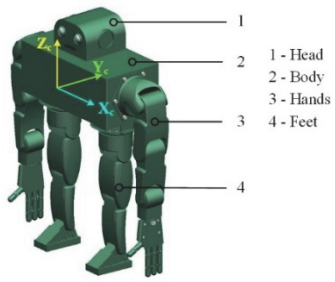

Figure 2 Model diagram of biped handling robot

To realize the designed bipedal robot's walking and handling functions, it is necessary to carry out the positive and inverse kinematics analysis of the hands and feet part. On this basis, the working process of carrying out the motion simulation is as follows.

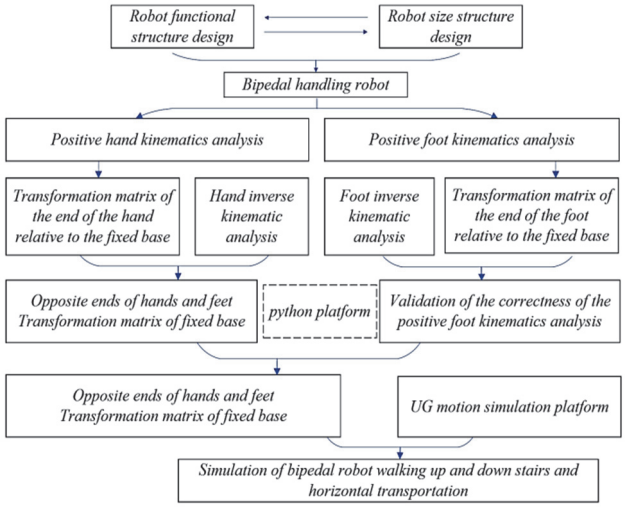

Figure 3 Main parameter diagram of bipedal handling robot

Firstly, the functional structure of the designed robot is constructed, and the geometric shape of the relevant structure is determined according to the mechanical design principle. Secondly, through the forward kinematics analysis of the robot designed by the hand and foot, the transformation matrix of the hand and foot end relative to the fixed seat is determined, and the correctness of the solution result is proved through the inverse kinematics analysis. The transformation matrix of the hand and foot end relative to the fixed seat is solved using Python platform.Finally, the results are distributed to the UG motion simulation platform, and the movements of the biped handling robot such as up and down stairs and horizontal walking are simulated and verified.

3 KINEMATIC ANALYSIS OF BIPEDAL HANDLING ROBOT

3.1 Kinematic Analysis of the Hand

The designed bipedal handling robot thumbs have only one degree of freedom, all other fingers have two degrees of freedom. Since the motion of the joint structures of the fingers is all the same, the motion analysis of only one finger is done. Considering that the finger joints are not independent movements, the following motion relations should be satisfied in the linkage [19].

$$\theta_i = 10\theta_{i0}\left(\frac{t}{t_0}\right)^3 - 15\theta_{i0}\left(\frac{t}{t_0}\right)^4 + 6\theta_{i0}\left(\frac{t}{t_0}\right)^5 \quad (1)$$

where, $i = 1, 2, 3$, represent the proximal, middle, and distal fingers, respectively; θ_{iO} is the angle turned by the three joints; t is time; and t_0 stands for the time spent for the whole motion. As both sides of the hand structure of the robot are identical in a mirror image distribution and their original state is perpendicular to the ground, the kinematic analysis is performed by the D-H method only for the overall motion of the unilateral hand.

3.1.1 Kinematic Analysis of the Hand

As mentioned above, the corresponding coordinate system for each joint is set in line with the right-hand rule (take the fixed coordinate system on the hand as reference, as shown in Fig. 4) . Joint 0 represents the rotation of the fixed base of the hand around the z axis of the relevant coordinate space, joint 1 stands the rotation of the large arm around the x axis of the relevant coordinate space, joint 2 claims the rotation of the small arm around the x axis of the relevant coordinate space, joint 3 means the rotation of the wrist around the x axis of the relevant coordinate space, joint 4 signifies the rotation of the wrist around the y axis of the relevant coordinate space, and joint 5 represents the end-effector. The coordinate parameters of each joint of the hand are shown in Tab. 1.

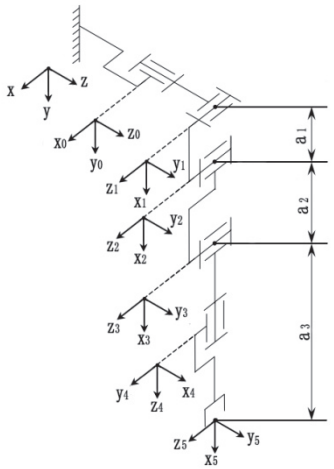

Figure 4 Coordinate system of each joint of biped handling robot hand

When joint 4 intersects the z axis of the end actuator (joint 5) in the actuator's coordinate system, the coordinates of the origin actuator of Joint 4 are transferred. The converted data is shown in Tab. 2.

Pay close attention that θ represents the angle of rotation around the z axis for the rotating joint where, $\alpha_1 = 150$ mm, $\alpha_2 = 150$ mm, $\alpha_3 = 312$ mm

Table 1 Hand D-H parameter

Joints	θ / °	α / °	a / mm	d / mm
1	θ_1	90	0	0
2	θ_2	0	α_1	0
3	θ_3	0	α_2	0
4	θ_4	90	0	0
5	θ_5	−90	α_3	0

Table 2 Hand D-H parameters

Joints	θ / °	α / °	a / mm	d / mm
1	θ_1	90	0	0
2	θ_2	0	α_1	0
3	θ_3	0	α_2	0
5	θ_5	0	α_3	0

From the data in Tab. 2, the coordinates matrices A_1 to A_4 of the associated joints are obtained, and then the final matrices of the arm rotation fixed base and the hand end (joint 5) of the bipedal handling robot.

$$
{}^0_4T = A_1A_2A_3A_4 = \begin{bmatrix} n_x & o_x & a_x & p_x \\ n_y & o_y & a_y & p_y \\ n_z & o_z & a_z & p_z \\ 0 & 0 & 0 & 1 \end{bmatrix} = \\
= \begin{bmatrix} C_1C_{235} & -C_1S_{235} & S_1 & C_1(a_3C_{235}+a_2C_{23}+a_1C_2) \\ S_1C_{235} & -S_1S_{235} & -C_1 & S_1(a_3C_{235}+a_2C_{23}+a_1C_2) \\ S_{235} & C_{235} & 0 & a_3S_{235}+a_2S_{23}+a_1S_2 \\ 0 & 0 & 0 & 1 \end{bmatrix} \tag{2}
$$

where, C_{15} denotes $C(\theta_1 + \theta_5)$, C_{123} denotes $C(\theta_1 + \theta_2 + \theta_3)$; S_{15} denotes, $S(\theta_1 + \theta_5)$, S_{123} denotes $S(\theta_1 + \theta_2 + \theta_3)$, and so on.

To ensure that the calculated results are correct, Eq. (2) is verified by performing four-by-four matrix operations (non-numerical) programmatically using Python software. Once the angles θ_1, θ_2, θ_3 and θ_5 of the hand joint are determined, the direction and coordinate posture of the end-effector (finger) can be obtained by Eq. (2) under the formulated relevant coordinate space.

3.1.2 Hand Inverse Kinematic Analysis

$$
A_1^{-1}\begin{bmatrix} n_x & o_x & a_x & p_x \\ n_y & o_y & a_y & p_y \\ n_z & o_z & a_z & p_z \\ 0 & 0 & 0 & 1 \end{bmatrix} = A_2A_3A_4 \tag{3}
$$

$$
\begin{bmatrix} C_1 & S_1 & 0 & 0 \\ 0 & 0 & 1 & 0 \\ S_1 & -C_1 & 0 & 0 \\ 0 & 0 & 0 & 1 \end{bmatrix} \times \\
\times \begin{bmatrix} C_1C_{235} & -C_1S_{235} & S_1 & C_1\left(a_3C_{235}+a_2C_{23}+a_1C_2\right) \\ S_1C_{235} & -S_1S_{235} & -C_1 & S_1\left(a_3C_{235}+a_2C_{23}+a_1C_2\right) \\ S_{235} & C_{235} & 0 & a_3S_{235}+a_2s_{23}+a_1S_2 \\ 0 & 0 & 0 & 1 \end{bmatrix} = \tag{4}
$$

$$
= \begin{bmatrix} S_{23}\left(C_5-S_5\right) & -S_{235} & 0 & a_3C_{235}+a_2C_{23}+a_1C_2 \\ S_{23}\left(C_5+S_5\right) & C_{235} & 0 & a_3S_{235}+a_2S_{23}+a_1S_2 \\ 0 & 0 & 1 & 0 \\ 0 & 0 & 0 & 1 \end{bmatrix}
$$

According to the elements of (3, 4) in Eq. (4) we have:

$$
p_xS_1 - p_yC_1 = 0 \tag{5}
$$

Rectifying Eq. (5) yields or:

$$
\theta_1 = \arctan\left(\frac{p_y}{p_x}\right) \text{ or } \theta_1 = \pi + \arctan\left(\frac{p_y}{p_x}\right) \tag{6}
$$

According to the elements (1, 2), (2, 2), (1, 4) and (2, 4) in Eq. (4) are:

$$
\begin{cases} o_xC_1 + o_yS_1 = -S_{235} \\ o_z = C_{235} \\ p_xC_1 + p_yS_1 = a_3C_{235} + a_2C_{23} + a_1C_2 \\ p_z = a_3S_{235} + a_2S_{23} + a_1S_2 \end{cases} \tag{7}
$$

Collating the third and fourth formulas in Eq. (7) and squaring both sides of the collated formula and adding them together gives:

$$
\left(p_xC_1 + p_yS_1 - a_3C_{235}\right)^2 + \left(p_z - a_3S_{235}\right)^2 \\
= a_1^2 + a_2^2 + 2a_1a_2\left(S_2S_{23} + C_2C_{23}\right) \tag{8}
$$

Rectifying Eq. (8) yields.

$$
C_3 = \frac{\left(p_xC_1 + p_yS_1 - a_3C_{235}\right)^2 + \left(p_z - a_3S_{235}\right)^2 - a_1^2 - a_2^2}{2a_1a_2} \tag{9}
$$

Then Eq. (7) is solved as follows:

$$
\begin{cases} \theta_{235} = \arctan\left(\dfrac{-o_xC_1 - o_yS_1}{o_z}\right) \\ \theta_3 = \arctan\dfrac{\pm\sqrt{1-C_3^2}}{C_3} \end{cases} \tag{10}
$$

According to the elements (1, 1) and (2, 1) in Eq. (4):

$$
\begin{cases} n_xC_1 + n_yS_1 = S_{23}\left(C_5 - S_5\right) \\ n_z = S_{23}\left(C_5 + S_5\right) \end{cases} \tag{11}
$$

Dividing Eq. (11) by the following equation to eliminate S_{23} and then sorting to obtain:

$$
\tan\theta_5 = \frac{n_z - n_xC_1 - n_yS_1}{n_z + n_xC_1 + n_yS_1} \tag{12}
$$

Then:

$$
\theta_5 = \arctan\left(\frac{n_z - n_xC_1 - n_yS_1}{n_z + n_xC_1 + n_yS_1}\right) \tag{13}
$$

From Eq. (10), Eq. (13), θ_{235}, θ_3 and θ_5 are known, from which it follows that:

$$
\theta_2 = \theta_{235} - \theta_3 - \theta_5 \tag{14}
$$

So the angles of the joints of the robot hand are as follows:

$$\begin{cases} \theta_1 = arctan\left(\dfrac{p_y}{p_x}\right) \ or \ \theta_1 = \pi + arctan\left(\dfrac{p_y}{p_x}\right) \\ \theta_{235} = \arctan\left(\dfrac{-o_x C_1 - o_y S_1}{o_z}\right) \\ C_3 = \dfrac{\left(p_x C_1 + p_y S_1 - a_3 C_{235}\right)^2 + \left(p_z - a_3 S_{235}\right)^2 - a_1^2 - a_2^2}{2a_1 a_2} \\ \theta_3 = \arctan\dfrac{\pm\sqrt{1-C_3^2}}{C_3} \\ \theta_5 = \arctan\left(\dfrac{n_z - n_x C_1 - n_y S_1}{n_z + n_x C_1 + n_y S_1}\right) \\ \theta_2 = \theta_{235} - \theta_3 - \theta_5 \end{cases} \quad (15)$$

Substituting $\theta_1 = \theta_2 = \theta_3 = \theta_5 = 0°$ initial state into Eq. (2) yields:

$$ {}^0_4T = A_1 A_2 A_3 A_4 = \begin{bmatrix} n_x & o_x & a_x & p_x \\ n_y & o_y & a_y & p_y \\ n_z & o_z & a_z & p_z \\ 0 & 0 & 0 & 1 \end{bmatrix} = \begin{bmatrix} 1 & 0 & 0 & (a_3 + a_2 + a_1) \\ 0 & 0 & -1 & 0 \\ 0 & 1 & 0 & 0 \\ 0 & 0 & 0 & 1 \end{bmatrix} \quad (16)$$

Note that the equation $[P_x\ P_y\ P_z]^{\mathrm{T}}$ is the end direction vector of the robot arm.

The calculation results of Eq. (16) are consistent with the results of the relative spatial position between the coordinate system as the starting position and the end actuator position in Fig. 4. The correctness of robot hand kinematics analysis is verified.

3.2 Kinematic Analysis of the Foot

The bipedal handling robot has a mirror-symmetric distribution of both feet centered on the body, with the original state of the body perpendicular to the ground. The structure and motion of both feet are identical, the overall motion of only one side of the foot can be kinematically analyzed using the D-H method.

3.2.1 Positive Kinematic Analysis of the Foot

The coordinates of the foot area (taking the fixed coordinate system set for the foot as a reference) are set with the same rules as the hand coordinates, which is shown in Fig. 5. Joint 0 shows the rotation of the fixed base of the foot around the z axis of the relevant coordinate system space, joint 1 represents the rotation of the thigh around the y axis of the relevant coordinate system space, joint 2 stands for the rotation of the lower leg around the y axis of the relevant coordinate system space, joint 3 means the rotation of the ankle around the y axis of the relevant coordinate system space, and joint 4 describes the end-effector. The coordinate parameters of each joint of the foot are shown in Tab. 3.

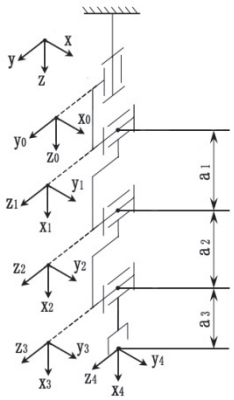

Figure 5 Coordinate system of each joint of the foot of the bipedal handling

Table 3 D-H parameter table of foot

Joint	θ / °	α / °	a / mm	d / mm
1	θ_1	−90	0	0
2	θ_2	0	α_1	0
3	θ_3	0	α_2	0
4	θ_4	0	α_3	0

Note that θ represents the angle of rotation around the z axis for the rotating joint where, a_1 = 150 mm, a_2 = 150 mm, a_3 = 58 mm.

From the data in Tab. 3, the coordinate matrices $A_1 \sim A_4$ between the two associated connections are obtained, and the final matrices of the rotating fixed base and the end of the foot of the bipedal handling robot are:

$$ {}^0_4T = A_1 A_2 A_3 A_4 = \begin{bmatrix} n_x & o_x & a_x & p_x \\ n_y & o_y & a_y & p_y \\ n_z & o_z & a_z & p_z \\ 0 & 0 & 0 & 1 \end{bmatrix} = \begin{bmatrix} C_1 C_{234} & -C_1 S_{234} & -S_1 & C_1(a_3 C_{234} + a_2 C_{23} + a_1 C_2) \\ S_1 C_{234} & -S_1 S_{234} & C_1 & S_1(a_3 C_{234} + a_2 C_{23} + a_1 C_2) \\ -S_{234} & -C_{234} & 0 & -\left(a_3 S_{234} + a_2 S_{23} + a_1 S_2\right) \\ 0 & 0 & 0 & 1 \end{bmatrix} \quad (17)$$

where, C_{13} denotes $C(\theta_1 + \theta_3)$, C_{123} denotes $C(\theta_1 + \theta_2 + \theta_3)$; S_{13} denotes, $S(\theta_1 + \theta_3)$, S_{123} denotes $S(\theta_1 + \theta_2 + \theta_3)$, and so on.

Eq. (17) is verified by performing four-by-four matrix operations (non-numerical) programmatically with Python software to guarantee the correct calculated results. Once the angles θ_1, θ_2, θ_3 and θ_4 of the foot joint are determined, the direction and coordinate relationship of the end-effector (foot) in a fixed coordinate system can be obtained by Eq. (17).

3.2.2 Foot Inverse Kinematic Analysis

Solving the angle according to the positive kinematic final position of total transformation matrix Eq. (17), multiplying the total transformation matrix by the left side of A_n^{-1} in turn, yields:

$$A_1^{-1}{}_4^0T=\begin{bmatrix} n_xC_1-n_yS_1 & o_xC_1-o_yS_1 & a_xC_1-a_yS_1 & p_xC_1-p_yS_1 \\ -n_z & -o_z & -a_z & -p_z \\ n_xS_1+n_yC_1 & o_xS_1+o_yC_1 & a_xS_1+a_xC_1 & p_xS_1+p_yC_1 \\ 0 & 0 & 0 & 1 \end{bmatrix}= \quad (18)$$

$$=\begin{bmatrix} S_{23}(C_4-S_4) & -S_{234} & 0 & a_3C_{234}+a_2C_{23}+a_1C_2 \\ S_{23}(C_4+S_4) & C_{234} & 0 & a_3S_{234}+a_2S_{23}+a_1S_2 \\ 0 & 0 & 1 & 0 \\ 0 & 0 & 0 & 1 \end{bmatrix}$$

According to the elements of (3, 4) in Eq. (17) there are:

$$p_xS_1+p_yC_1=0 \quad (19)$$

Rectifying Eq. (19) yields:

$$\theta_1=\arctan\left(-\frac{p_y}{p_x}\right) \text{ or } \theta_1=\pi+\arctan\left(-\frac{p_y}{p_x}\right) \quad (20)$$

According to the elements (1, 2), (2, 2), (1, 4) and (2, 4) in Eq. (17) are:

$$\begin{cases} o_xC_1-o_yS_1=-S_{234} \\ -o_z=C_{234} \\ p_xC_1-p_yS_1=a_3C_{234}+a_2C_{23}+a_1C_2 \\ -p_z=a_3S_{234}+a_2S_{23}+a_1S_2 \end{cases} \quad (21)$$

In the third and fourth formulas in the collating Eq. (21) square the two sides of the collating formula and add them up to:

$$\begin{aligned} &\left(p_xC_1-p_yS_1-a_3C_{234}\right)^2+\left(p_z+a_3S_{234}\right)^2 \\ &=a_1^2+a_2^2+2a_1a_2\left(S_2S_{23}+C_2C_{23}\right) \end{aligned} \quad (22)$$

Rectify Eq. (22) to obtain:

$$C_3=\frac{\left(p_xC_1-p_yS_1-a_3C_{234}\right)^2+\left(p_z+a_3S_{234}\right)^2-a_1^2-a_2^2}{2a_1a_2} \quad (23)$$

Then the Eq. (21) is solved for.

$$\begin{cases} \theta_{234}=\arctan\left(\dfrac{o_xC_1-o_yS_1}{o_z}\right) \\ \theta_3=\arctan\dfrac{\pm\sqrt{1-C_3^2}}{C_3} \end{cases} \quad (24)$$

According to the elements (1,1) and (2,1) in Eq. (17) we have:

$$\begin{cases} n_xC_1-n_yS_1=S_{23}\left(C_4-S_4\right) \\ -n_z=S_{23}\left(C_4+S_4\right) \end{cases} \quad (25)$$

Dividing Eq. (25) by the following equation eliminates S_{23}, and then collapses to obtain the relationship:

$$\tan\theta_4=\frac{n_z-n_xC_1-n_yS_1}{n_z+n_xC_1+n_yS_1} \quad (26)$$

Therefore, θ_4 can give the following:

$$\theta_4=\arctan\left(\frac{n_z+n_xC_1-n_yS_1}{n_z-n_xC_1+n_yS_1}\right) \quad (27)$$

By means of Eq. (24) and Eq. (26) is known θ_{234}, θ_3 and θ_4, from which it follows that:

$$\theta_2=\theta_{234}-\theta_3-\theta_4 \quad (28)$$

the angle of each joint of the robot foot is:

$$\begin{cases} \theta_1=arctan\left(-\dfrac{p_y}{p_x}\right) \text{ or } \theta_1=\pi+arctan\left(-\dfrac{p_y}{p_x}\right) \\ \theta_{234}=\arctan\left(\dfrac{o_xC_1-o_yS_1}{o_z}\right) \\ C_3=\dfrac{\left(p_xC_1-p_yS_1-a_3C_{234}\right)^2+\left(p_z+a_3S_{234}\right)^2-a_1^2-a_2^2}{2a_1a_2} \\ \theta_3=\arctan\dfrac{\pm\sqrt{1-C_3^2}}{C_3} \\ \theta_4=\arctan\left(\dfrac{n_z+n_xC_1-n_yS_1}{n_z-n_xC_1+n_yS_1}\right) \\ \theta_2=\theta_{234}-\theta_3-\theta_4 \end{cases} \quad (29)$$

Substituting $\theta_1=\theta_2=\theta_3=\theta_4=0°$ initial state into Eq. (17) gives:

$$\begin{aligned} {}_4^0T=A_1A_2A_3A_4&=\begin{bmatrix} n_x & o_x & a_x & p_x \\ n_y & o_y & a_y & p_y \\ n_z & o_z & a_z & p_z \\ 0 & 0 & 0 & 1 \end{bmatrix}= \\ &=\begin{bmatrix} 1 & 0 & 0 & (a_3+a_2+a_1) \\ 0 & 0 & 1 & 0 \\ 0 & -1 & 0 & 0 \\ 0 & 0 & 0 & 1 \end{bmatrix} \end{aligned} \quad (30)$$

Note that the formula $[P_x\ P_y\ P_z]^T$ is the end direction vector of the robot arm.

The result of Eq. (30) maps to the coordinate system of Fig. 5 state from the connection 1 as the start to the end-effector position. The correctness of the foot kinematic analysis is demonstrated.

4 SIMULATION

In this paper, the simulated motion place of the bipedal handling robot is located in a staircase to meet the requirement of smooth handling up and down stairs assigning the angle of each joint of the robot by the Step function, giving the robot to adjust the magnitude of the movement of going up and down the stairs and the

movement of lifting heavy objects in real time from the inverse kinematics derivation Eq. (15), Eq. (29) under the UGNX12.0 simulation environment. The simulation time is 57 s, the number of steps is 51, the distance of each step is the width of the front and back of the stairs, the height of each step is the height of the stairs, the number of steps required to climb the stairs is 20, the number of steps on the horizontal plane is 16, and the number of steps required to go down the stairs is 15. By the single person single wall staircase size standard is roughly the width of the staircase section between 750 mm and 900 mm. The width of the stair tread before and after should not be less than 200 mm and the height should not be greater than 175 mm [15-16]. In order to observe the simulated handling simulation, it is assumed that the robot walks up and down in an environment that satisfies the conditions of a single-person building (five steps), and the width of each stairway section is 750 mm on the left and right, 200 mm on the front and back, and 80 mm on the height, and the items carried by the bipedal handling robot are replaced by rectangular bodies. The time required for each stage is calculated as follows.

(1) Time required for climbing the stairs.In the process of climbing stairs, the robot bends its fingers to avoid interference with the ground when walking, and then alternates between the left and right feet, keeping the soles of the feet parallel to the ground, with each gait action time t_1 set to 1s, finishing a step with four gait i_1, i.e. b-c-d-e/e-f-g-b as shown in Fig. 6, with the robot moving a distance S_1 of 200 mm. The number of steps n to be walked for a step height h of 80 mm is 5. The total height L of the robot walking platform to the platform of the desired item to be moved is:

$$L = h \times n = 400 \text{ mm} \tag{31}$$

T_1 for the robot to go up the stairs to reach the platform for carrying the item gives that:

$$T_1 = \frac{L}{h} \times t_1 \times i_1 = 20 \text{ s} \tag{32}$$

(2) Time required for walking on a horizontal plane of the stairs： In the process of walking on the horizontal plane of the stairs, the robot uses two gait i_2 of lifting foot and landing to complete a forward progress, and the time t_2 set to 1 s, the robot moving distance S_2 is 200 mm, due to consideration of space no longer do the diagram. When the robot arrives near the object to be moved, it restores its upright form, and then drives the body and hands to carry. The total time t_p required by the robot in the process of stopping and lifting is 6 s. The width d of the platform from which the item is placed is 1600 mm. the robot carries the item until it goes downstairs, then the time required T_2 is:

$$T_2 = \frac{d}{S_2} \times t_2 \times i_2 + t_p = 22 \text{ s} \tag{33}$$

(3) Time required for climbing down the stairs: The robot maintains the law of alternating cooperation between the left and right feet, and the sole of the foot remains parallel to the ground, with three gait i_3 (single foot off the ground foot up landing) to complete a step action, its time t_3 is set to 1s. Due to the consideration of space, no illustration will be made. The time required for the robot to take articles down the stairs T_3 is.

$$T_3 = \frac{L}{h} \times t_3 \times i_3 = 15 \text{ s} \tag{34}$$

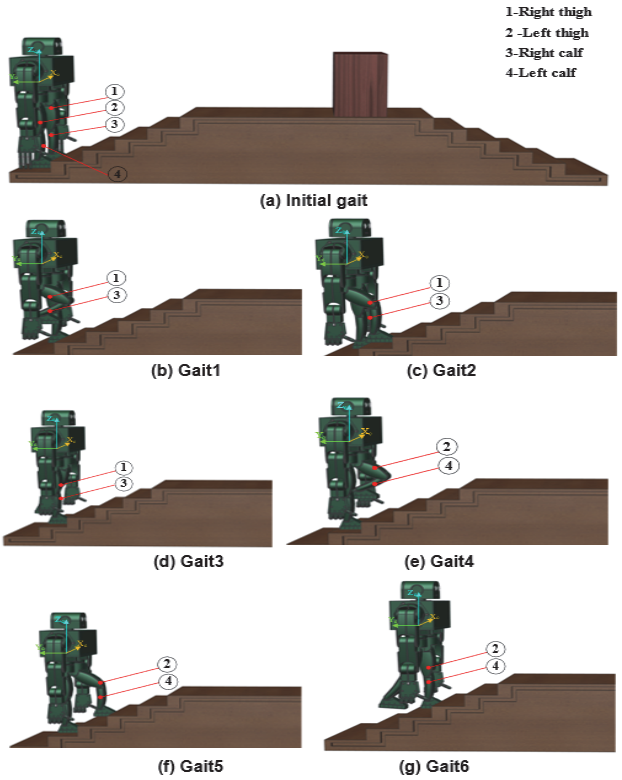

Figure 6 Example of walking up stairs

In the UG NX simulation environment, the negative direction of y-axis is used as the forward direction to simulate the three states of the bipedal handling robot going upstairs, parallel forward carrying items and going downstairs. These three states with continuous movements are shown in Fig. 7.

Fig. 7a shows the displacement of the robot in the forward direction in three consecutive states, which shows the displacement of the robot in the three states respectively.

Fig. 7b shows the velocity diagram of the forward direction in three consecutive states of the handling robot, and the velocity has positive and negative directions because the foot belongs to the oscillating motion when walking. In between the gait changes the robot will have a sudden change of movement that is between the horizontal ground and the road with height, at this time there will be sudden fluctuation of speed but displacement changes without obvious cliff jump, such as Fig. 7b 42 s – 57 s, so it does not affect the normal walking of the robot.

The motion of the bipedal robot in these three states did not show any abnormal conditions such as stalling, instability and shaking, and the motion pattern was stable without sudden changes, which proved that the robot could achieve the transport motion.

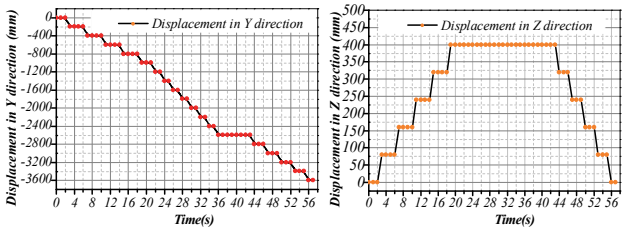

(a) The displacement curve diagram of the biped carrying robot's forward direction

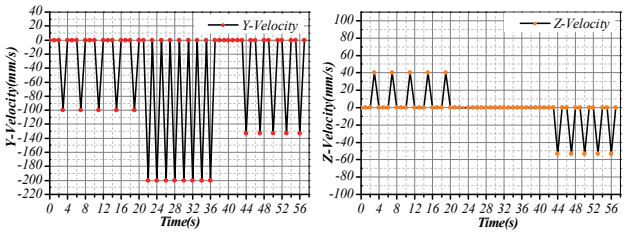

(b) The speedt curve diagram of the biped carrying robot's forward direction

Figure 7 Simulation results of foot movement of biped handling robot

5 CONCLUSION

Based on the developed and designed bipedal handling robot model, the kinematics related data operation is carried out by combining Python with the known angle and motion relationship of each rigid body to carry out the derivation of positive and inverse kinematics, and the motion simulation calculation of the bipedal handling robot is carried out based on UG motion simulation with the kinematics analysis, and the results show the following:

(1) the inverse kinematics solution is implemented in Python, and the motion of the bipedal handling robot is analyzed by the D-H method, the possibility of its motion states and the motion relationship between each rigid body are proved to be correct.

(2) In the simulation of the motion of the bipedal transport robot, the angle control makes the bipedal parts alternate with each other to realize the smooth forward motion of the bipedal transport robot. The motion simulation shows that the speed of the foot down is slower in the process of going up the stairs, moving horizontally and going down the stairs, and the speed of going down the stairs is faster than going up the stairs.

(3) The motion simulation results of the bipedal transport robot show that the running speed of the bipedal transport robot has a small change along the horizontal direction in the running process, and the change of speed when going down the stairs is larger than the change of speed when going up the stairs and moving horizontally, but it does not affect the motion and meets the design requirements.

The analysis and simulation of the bipedal handling robot confirmed more possibilities and practicality for robot diversification, and provided a referenceable theoretical basis and ideas for further research on intelligent products of the bipedal handling class.

Acknowledgement

Fund project: National Natural Science Foundation of Guangdong Province (2021A1515010533), Guangzhou City Science and Technology Project (202201011603).

6 REFERENCES

[1] Nishida, T., Takemura, Y., Fuchikawa, Y., Kurogi, S., Ito, S., Obata, M., & Ohkawa, F. (2006). Development of outdoor service robots. *In 2006 SICE-ICASE International Joint Conference*, 2052-2057. https://doi.org/10.1109/SICE.2006.315491

[2] *Biomimetic Robots Market World Technology, Development Status, Industry Size & Share, Segments and Forecasts 2018-2023*. M2 Presswire, 2018.

[3] Lei, J. T., Yu, H. Y., & Wang, T. M. (2016). Dynamic bending of bionic flexible body driven by pneumatic artificial muscles(PAMs) for spinning gait of quadruped robot. *Chinese Journal of Mechanical Engineering*, *29*(01), 11-20. https://doi.org/10.3901/CJME.2015.1016.123

[4] Qiao, T. B. (2020). Gait control of hexapod robot based on field-programmable gate array and central pattern generator. *Journal Européen des SystèmesAutomatisés, 53*(6), 931-937. https://doi.org/10.18280/jesa.530619

[5] Wang, T. M., Tao, Y., & Liu, H. (2018). Current researches and future development trend of intelligent robot: a review.*International Journal of Automation and Computing*, *15*(05), 525-546. https://doi.org/10.1007/s11633-018-1115-1

[6] Yang, L. L. (2019). An attitude motion planning algorithm for one-legged hopping robot based on spline approximation and particle swarm optimization. *Revue d'Intelligence Artificielle*, *33*(1), 49-52. https://doi.org/10.18280/ria.330109

[7] Abed, M. S., Lutfy, O. F., & Al-Doori, Q. F. (2022). Online path planning of mobile robots based on African vultures optimization algorithm in unknown environments. *Journal Européen des SystèmesAutomatisés*, *55*(3), 405-412. https://doi.org/10.18280/jesa.550313

[8] Lv, M. Y., Li, J. Q., & Fu, R. (2012). A Palletizing Robot Dynamics Analysis. *International Journal of Advancements in Computing Technology*, *4*(11), 398-404. https://doi.org/10.4156/ijact.vol4.issue11.43

[9] Song, L. Z., Zhu, J., Liu, S. T., & Qu, Z. J. (2022). Recent Fire Safety Design of High-Rise Buildings. *Journal of Urban Development and Management*, *1*(1), 50-57. https://doi.org/10.56578/judm010106

[10] Pham, T. T., Le, M. T., & Nguyen, C. N. (2021). Omnidirectional mobile robot trajectory tracking control with diversity of inputs. *International Journal of Mechanical Engineering and Robotics Research*, *10*(11), 639-644. https://doi.org/10.18178/ijmerr.10.11.639-644

[11] Boukheddimi, M., Bailly, F., Souères, P., & Watier, B. (2019). Human gait simulation from a reduced set of low-dimensional tasks using hierarchical control. *Computer Methods in Biomechanics and Biomedical Engineering*, *22*(sup1), S408-S410. https://doi.org/10.1080/10255842.2020.1714962

[12] Weiwei, Z. (2020). Finite element static analysis of main arm for a special manipulator. *In Journal of Physics: Conference Series*, *1676*(1), 012145. https://doi.org/10.1088/1742-6596/1676/1/012145

[13] Mallik, A. K., Ghosh, A., & Dittrich, G. (2021). Kinematic analysis and synthesis of mechanisms. *Crc Press*. https://doi.org/10.1201/9780429327278

[14] Liu, Y. X., Zou, S. L., He, Z. F., & Zhang, D. (2013). Design on Manipulator Hand Structure Working in the Radiation Environment. *In Advanced Materials Research*, *807*, 1376-1379. https://doi.org/10.4028/www.scientific.net/AMR.807-809.1376

[15] de Santos, P. G., Garcia, E., Sarria, J., Ponticelli, R., & Reviejo, J. (2010). A new manipulator structure for power-assist devices. *Industrial Robot: An International Journal*, *37*(5), 452-458. https://doi.org/10.1108/01439911011063272

[16] Bangash, M. Y. H. & Bangash, T. (2019). Staircases: structural analysis and design. *Routledge*. https://doi.org/10.1201/9780203738801

[17] Hasan, S. K. & Dhingra, A. K. (2021). Development of a model reference computed torque controller for a human lower extremity exoskeleton robot. *Proceedings of the Institution of Mechanical Engineers, Part I: Journal of Systems and Control Engineering*, *235*(9), 1615-1637. https://doi.org/10.1177/09596518211009032

[18] Samuel, A. U., Araoyinbo, A. O., Elewa, R. R., & Biodun, M. B. (2021, April). Effect of machining of aluminium alloys with emphasis on aluminium 6061 alloy-a review. *IOP Conference Series: Materials Science and Engineering*, *1107*(1), 012157. https://doi.org/10.1088/1757-899X/1107/1/012157

[19] Liu, X., Zheng, X., & Li, S. (2017). Development of a humanoid robot hand with coupling four-bar linkage. *Advances in Mechanical Engineering*, *9*(1), 1687814016686313. https://doi.org/10.1177/1687814016686313

[20] Ozawa, R. & Tahara, K. (2017). Grasp and dexterous manipulation of multi-fingered robotic hands: a review from a control view point. *Advanced Robotics*, *31*(19-20), 1030-1050. https://doi.org/10.1080/01691864.2017.1365011

Contact information:

Zhen Yu TANG, Associate Professor
The School of Naval Architecture and Ocean Engineering,
Guangzhou Maritime University,
Guangzhou, China
E-mail: tangzhenyu@gzmtu.edu.cn

Qi Lin BI, Associate Professor
(Corresponding author)
The School of Naval Architecture and Ocean Engineering,
Guangzhou Maritime University,
Guangzhou, China
E-mail: bi.qilin@mail.scut.edu.cn

Xue Min NING
Shenzhen Dazu Precision Transmission Technology Co.Ltd,
Shenzhen, Chnia
E-mail: ning_xuemin@foxmail.com

Lun TANG
Guangdong Navigation Association,
Guangzhou 730050, China
E-mail: tanglun020@foxmail.com

Minling LAI
Guangdong Technology University,
Guangzhou, Guang Dong, China
E-mail: minling.lai@foxmail.com

Jindong YU, Associate Professor
The School of Naval Architecture and Ocean Engineering,
Guangzhou Maritime University,
Guangzhou, China
E-mail: yujdemail@qq.com